Imajo *et al. Earth, Planets and Space* (2016) 68:137
DOI 10.1186/s40623-016-0514-1

Earth, Planets and Space

FULL PAPER Open Access

Solar terminator effects on middle- to low-latitude Pi2 pulsations

Shun Imajo[1*], Akimasa Yoshikawa[1], Teiji Uozumi[2], Shinichi Ohtani[3], Aoi Nakamizo[4], Sodnomsambuu Demberel[5] and Boris Mikhailovich Shevtsov[6]

Abstract

To clarify the effect of the dawn and dusk terminators on Pi2 pulsations, we statistically analyzed the longitudinal phase and amplitude structures of Pi2 pulsations at middle- to low-latitude stations (GMLat = 5.30°–46.18°) around both the dawn and dusk terminators. Although the *H* (north–south) component Pi2s were affected by neither the local time (LT) nor the terminator location (at 100 km altitude in the highly conducting *E* region), some features of the *D* (east–west) component Pi2s depended on the location of the terminator rather than the LT. The phase reversal of the *D* component occurred 0.5–1 h after sunrise and 1–2 h before sunset. These phase reversals can be attributed to a change in the contributing currents from field-aligned currents (FACs) on the nightside to the meridional ionospheric currents on the sunlit side of the terminator, and vice versa. The phase reversal of the dawn terminator was more frequent than that of the dusk terminator. The *D*-to-*H* amplitude ratio on the dawn side began to increase at sunrise, reaching a peak approximately 2 h after sunrise (the sunward side of the phase reversal region), whereas the ratio on the dusk side reached a peak at sunset (the antisunward side). The dawn–dusk asymmetric features suggest that the magnetic contribution of the nightside FAC relative to the meridional ionospheric current on the dusk side is stronger than that on the dawn side, indicating that the center of Pi2-associated FACs, which probably corresponds to the Pi2 energy source, tends to be shifted duskward on average. Different features and weak sunrise/sunset dependences at the middle-latitude station (Paratunka, GMLat = 46.18°) can be attributed to the larger annual variation in the sunrise/sunset time and a stronger magnetic effect because of closeness from FACs. The *D*-to-*H* amplitude ratio decreased with decreasing latitude, suggesting that the azimuthal magnetic field produced by the FACs in darkness and the meridional ionospheric current in sunlight also decreased with decreasing latitude.

Keywords: Geomagnetic pulsations, Pi2 pulsation, Ionospheric current system, Solar terminator, Dawn–dusk asymmetries

Background

Pi2 pulsations are irregular and short-duration geomagnetic oscillations with a period of 40–150 s (Jacobs et al. 1964; Saito 1964). Although the source (or the energy source) of Pi2 is believed to be localized in the magnetotail region (e.g., Uozumi et al. 2007; Chi et al. 2009; Keiling et al. 2014), Pi2 pulsations have been observed in low-latitude and equatorial regions on the dayside ground (e.g., Yanagihara and Shimizu 1966; Kitamura et al. 1988; Sutcliffe and Yumoto 1989). The amplitude of dayside Pi2 is enhanced near the magnetic equator, in a way similar to other disturbances that propagate from a source in the magnetosphere (e.g., Yanagihara and Shimizu 1966; Sastry et al. 1983; Shinohara et al. 1997). Therefore, in order to understand the propagation mechanism of Pi2 toward the dayside and the equatorial enhancement, it is important to study Pi2 pulsations observed in the dawn and dusk regions that mark the transition between nightside and dayside.

One of the most notable features of the dawn and dusk regions is a strong longitudinal gradient of the

*Correspondence: imajo@kyudai.jp
[1] Department of Earth and Planetary Sciences, Kyushu University, 744 Motooka, Nishi-ku, Fukuoka 819-0395, Japan
Full list of author information is available at the end of the article

ionospheric conductivity near the solar terminator. This feature alters the patterns of ionospheric currents and the magnetic field on the ground which is driven by those currents. The effects of the dawn terminator on Pc-type geomagnetic pulsations have been studied by several authors (Saka et al. 1980, 1982, 1988; Saka and Alperovich 1993; Alperovich et al. 1996; Tanaka et al. 2004, 2007). Their results show that some of the features of Pc-type geomagnetic pulsations are determined by the location of the terminator.

There have been far fewer studies of terminator effects on Pi pulsations than on Pc pulsations. Saka et al. (1980) observed Pi2 and Pc4 period range pulsations at the single station ASO (GMLat = 22°) near the dawn terminator. They found that an increase in the *D*-to-*H* (east-west to north-south) amplitude ratio occurred simultaneously with *E* layer ionization at sunrise. Imajo et al. (2015) presented case studies of Pi2 pulsations simultaneously observed at multiple low-latitude stations (L = 1.15–2.33) around the dawn terminator. They found that the *D* component oscillations in the dark and sunlit hemispheres were in antiphase, whereas the *H* component oscillated in phase. To clarify the significance and effect of the terminator, statistically robust comparisons should be made between the longitudinal structures based on the location of the terminator and local time (LT) dependences. Imajo et al. (2015) analyzed only the *D* component phase structure at the ASB station (GMLat = 36.43°) on the dawn side using such a statistical analysis.

Dusk terminator effects on geomagnetic pulsations are less well understood than dawn terminator effects. If only a sharp gradient of conductivities is considered, the terminator effects are almost the same at dawn and dusk. However, case studies by Imajo et al. (2015) showed that the distributions of wave properties with respect to the location of the terminators are not the same, although similar *D* component phase reversals were also found on the dusk side. A more detailed understanding of the differences between the effects of dawn and dusk terminators may provide clues to the determination of geometrical differences in currents.

The equatorial enhancement of dayside Pi2 suggests that ionospheric currents play an important role in propagation from nightside to dayside. The sources of the ionospheric electric fields associated with Pi2, which are thought to be field-aligned currents (FACs), are typically located at high latitudes (Shinohara et al. 1998). Yoshikawa et al. (2012) suggested that the meridional ionospheric current near the terminator connected the high-latitude FACs to the equatorial Cowling current, and Imajo et al. (2015) applied such current closure to Pi2 pulsations. The morphology of the meridional ionospheric current can be understood by investigating the latitudinal variation in the terminator effects.

In this research, we conduct a statistical analysis of the longitudinal phase and amplitude structures of Pi2 pulsations at middle- to low-latitude stations (GMLat = 5.30°–46.18°) around both the dawn and dusk terminators. Dependences on sunrise/sunset reference times (the time measured from the dawn/dusk terminator) at each station are compared with those on LT (the time as measured from the midnight meridian). We discuss the mechanisms and geometries that explain the longitudinal and latitudinal structures of Pi2, which are controlled by a sharp gradient in ionospheric conductivity near the terminator.

Methods

Data description

The coordinates of the stations used in this paper are listed in Table 1. PTK, ASB, and HVD are MAGDAS/CPMN [MAGnetic Data Acquisition System/Circumpan Pacific Magnetometer Network (Yumoto and the MAGDAS Group 2006, 2007)] stations, KAK and CBI are JMA (Japan Meteorological Agency) stations, TUC and GUA are USGS (US Geological Survey) stations, and TAM is a BCMT (Bureau Central de Magnetisme Terrestre) station. We examine Pi2 pulsations observed at the five magnetometer stations separated in latitude along the similar meridian (PTK, ASB, KAK, CBI, and GUA stations). The HVD station was used as the reference station for examining the change of phase. Figure 1 is a map of the stations, including the reference station. The differences in LT between the reference station and the test stations ranged from 3.2 to 4.4 h. The TAM and TUC stations were used in visual inspection for event selection as reference stations for identifying the nightside Pi2. A time resolution of 1 s was used, and in the local magnetic coordinate system (*HDZ* coordinates) the *H* component was local magnetic north, the *D* component was local magnetic east, and the *Z* component was downward.

Event selection

Pi2 events were identified from ASB data using both automatic detection and visual inspection. For the automatic detection of Pi2-like wave packets, the original data from ASB were converted to a time-series of Pi2 wave energy (Uozumi et al. 2000) with an envelope of $\Delta H^2 + \Delta D^2$ (where ΔH and ΔD are band-pass-filtered H and D, respectively, in the period range from 40 to 150 s). The use of both the H and D components enabled us to evaluate the amplitude of Pi2 without referencing change in polarization. A Pi2-like wave packet was based on the following criteria:

Table 1 The geographic and geomagnetic location of each station

Station code	Geographic latitude	Geographic longitude	Geomagnetic latitude	Geomagnetic longitude	L
MAGDAS/CPMN					
HVD	48.01	91.67	43.51	164.05	1.90
PTK	52.94	158.25	46.17	226.02	2.12
ASB	43.46	142.17	36.43	213.39	1.54
JMA					
KAK	36.23	140.19	27.47	209.23	1.26
CBI	27.10	142.19	18.58	212.10	1.11
USGS					
TUC	32.17	249.27	39.84	314.19	1.78
GUA	13.59	144.87	5.30	215.64	1.03
BCMT					
TAM	22.79	5.53	9.22	78.37	1.03

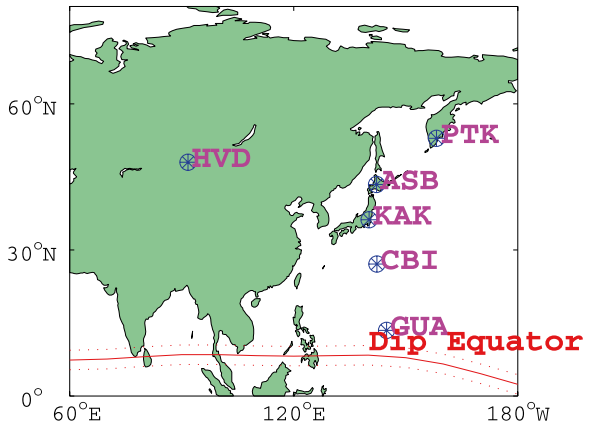

Fig. 1 Map of the test stations and reference station HVD

(1) The peak in the wave energy must exceed 0.0625 nT^2, where the time of the peak is defined as the event time (T_{max}).
(2) The wave energy at T_{max} must reach a maximum in the interval from 10 min before T_{max} to 10 min after T_{max}.
(3) The wave energy in the interval of $T_{max} - 7$ min to $T_{max} - 2$ min is used to confirm that the amplitude of the background disturbance is significantly smaller than that of Pi2. The average wave energy in this interval must be less than 5 % of the wave energy at T_{max}.

Events displaying the following background variations were removed by visual inspection: (1) spike-like and step-like artificial noise, (2) step-like variations with sudden commencements and sudden impulses, and (3) Pc4-like continuous waves. However, in some cases it remained difficult to distinguish between Pi2 and Pc4 on the dayside. In such cases, we referred to the magnetic data from the nightside station (TAM for dawn side events and TUC for dusk side events) and removed any events that had no clear Pi2 signature in the nightside data.

Pi2 events were selected from the period from November 1, 2011 to October 31, 2012, for which large amounts of data were available. We selected a total of 213 Pi2 events on the dawn side (between 0100 and 0900 LT at ASB) and 167 Pi2 events on the dusk side (between 1300 and 2100 LT at ASB).

Calculation of phase lag and amplitude

To obtain the phase lag between two Pi2 waves, we used a cross-phase analysis. The squared coherence (C_{xy}^2) and phase lag (θ_{xy}) can be written as functions of the frequency f as follows:

$$C_{xy}(f)^2 = \frac{|S_{xy}(f)|^2}{S_{xx}(f)S_{yy}(f)}, \tag{1}$$

$$\theta_{xy}(f) = \arctan\frac{\Im(S_{xy}(f))}{\Re(S_{xy}(f))} \tag{2}$$

where $S_{xx}(f)$ and $S_{yy}(f)$ are the power spectra of the test and reference data, respectively, and $S_{xy}(f)$ is the cross-spectrum of these data. Before calculating the spectra, we applied a Butterworth band-pass filter with a range of 10–300 s to the original data to attenuate the background trend and high-frequency noise. We calculated these spectra using Welch's modified periodogram method (Welch 1967). The spectral components were calculated for an interval from 3 min before to 7 min after T_{max} (600 samples). The phase lag and squared coherence of Pi2

were determined at the dominant frequency (f_d), which is the maximum peak of $S_{xx}(f)$ in the frequency range from 6 to 22 mHz. The phase lag and squared coherence between the two Pi2 waves were derived as $\theta_{xy}(f_d)$ and $C_{xy}(f_d)^2$, respectively. The phase lag is reliable only when the coherence is high. To reduce the error of the phase lag, we used values of $\theta_{xy}(f_d)$ in which $C_{xy}(f_d)^2$ was greater than 0.95.

An example of the application of this cross-phase analysis is given in Fig. 2 (20:09:02–20:19:02 UT, August 24, 2012 event). It can be seen that the waveforms exhibited a 180° phase lag from the band-pass-filtered data (a). The dominant frequency (f_d) shown by the vertical line was 12 mHz (b). $C_{xy}(f_d)^2$ was 0.99 (c), so $\theta_{xy}(f_d)$ had a reliable value of −175.9° (d), which was consistent with the phase lag visually determined from the waveforms.

Sunrise and sunset reference times

In this research, sunrise and sunset were defined as the times when the center of the Sun appeared above the horizon at dawn and dusk, respectively. We adopted sunrise/sunset reference times (ΔT_{sr}(STN)/ΔT_{ss}(STN)) [hours] as measures of the location of a station STN (the code for an arbitrary station) relative to the dawn/dusk terminator. The sunrise/sunset reference time was defined as the difference between the sunrise/sunset time in UT at each station at 100 km in altitude and the event time. For ΔT_{sr}(STN), negative values indicate that the station was in darkness, while positive values indicate that the station was in sunlight. For ΔT_{ss}(STN), negative values indicate that the station was in sunlight, while positive values indicate that the station was in darkness.

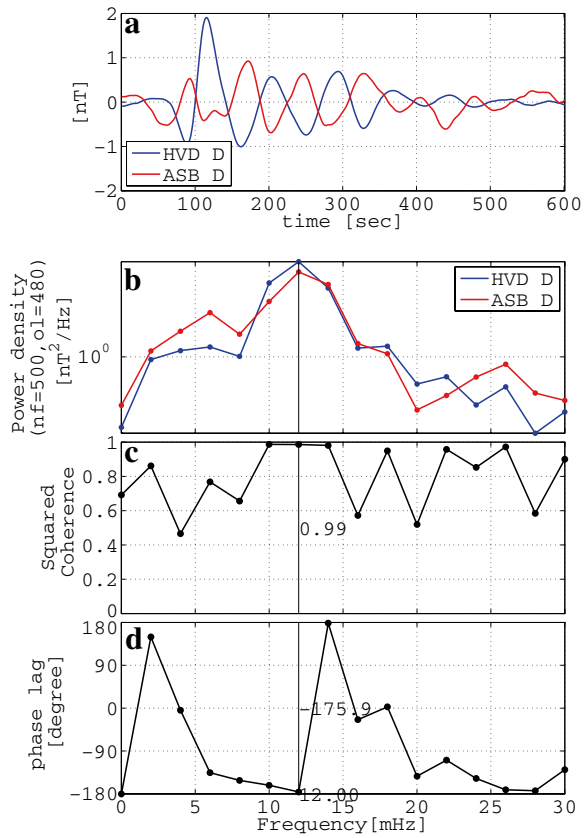

Fig. 2 An example application of the cross-phase analysis (20:09:02–20:19:02 UT, August 24, 2012 event). **a** Analyzed data band-pass-filtered with a period range of 10–300 s. **b** Power spectrum density ($S_{xx}(f)$,$S_{yy}(f)$). **c** Squared coherence ($C_{xy}(f)^2$). **d** Phase lag ($\theta_{xy}(f)$)

Results

Pi2 around the dawn terminator

Figure 3 presents the LT and ΔT_{sr} dependences of the phase lag of the *H* component between HVD and the five test stations. Positive values indicate that the phase of the reference data (HVD *H*) was delayed with respect to the test data. The color-coded dots indicate the location of the HVD station with respect to the $\Delta T_{sr}(\mathrm{HVD}) = 0.5$; blue dots show events satisfying $\Delta T_{sr}(\mathrm{HVD}) \leq 0.5$, and red dots show events satisfying $\Delta T_{sr}(\mathrm{HVD}) \geq 0.5$. The red and cyan vertical lines show the sunrise times at the summer and winter solstices. It is clear that most phase lags were close to 0° for both LT and ΔT_{sr} and for all stations except PTK. The phase lag at PTK *H* was more scattered, but the phase of HVD was delayed with respect to that at PTK.

Figure 4 shows the LT and ΔT_{sr} dependences of the phase lag of the *D* component between HVD and the five test stations. The phase lags at ASB, KAK, and CBI showed a clear phase shift from ∼0° to ∼180° near ΔT_{sr} = 0.5–1, whereas there was no clear systematic change of phase with LT. These results suggest that the phase reversal of the *D* component was related to the location of the dawn terminator rather than to the LT. Except for PTK, the phase lags for $\Delta T_{sr} \leq -1$ were more scattered, which may be attributable to a smearing of the phase reversal around midnight. The LT and ΔT_{sr} dependences at GUA were similar because of the small yearly variation in sunrise time. Although the phase lag was scattered for $\Delta T_{sr}(\mathrm{GUA}) \leq 1$, the phase lag for $\Delta T_{sr}(\mathrm{GUA}) \geq 1$ was close to 180°, as was that for $\Delta T_{sr}(\mathrm{PTK}) \leq -1$. Since the LT at PTK for $\Delta T_{sr}(\mathrm{PTK}) \leq -1$ was near midnight in the summer season, these antiphase relations may be caused by a near-midnight phase reversal associated with substorm current wedge oscillation (Lester et al. 1983) or a node of the cavity mode resonance (Allan et al. 1996). Although the number of events satisfying $\Delta T_{sr}(\mathrm{HVD}) \geq 0.5$ (red dots) is small, the phase difference shows a jump from 180° to 0° with respect to the change of dot color. This means the crossing of the phase

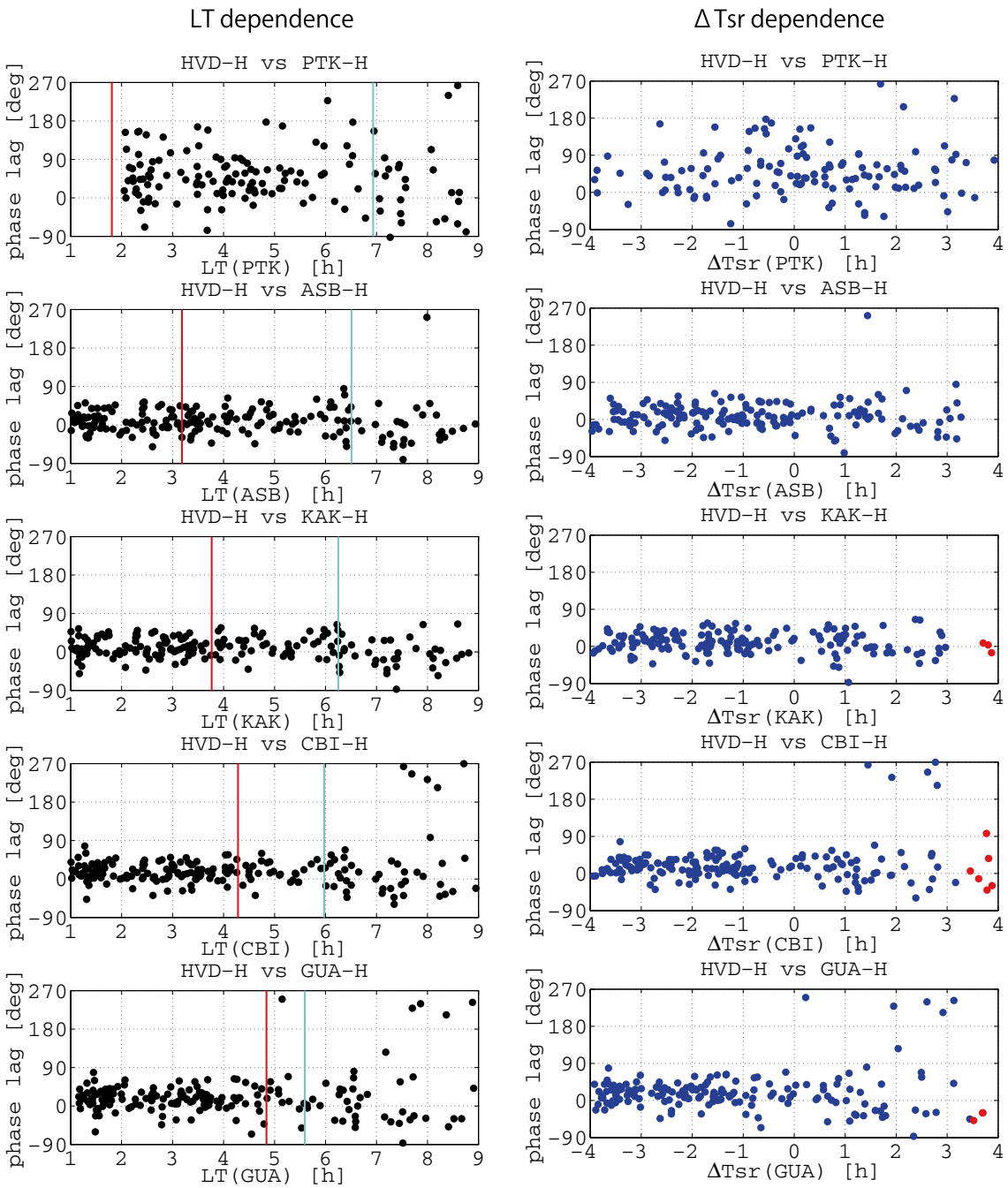

Fig. 3 LT and ΔT_{sr} dependency of the phase lag of the *H* component between HVD and the five test stations. *Positive values* indicate that the phase of test data was delayed with respect to the reference data. The *color-coded dots* indicate the location of the HVD station with respect to the $\Delta T_{sr}(\mathrm{HVD}) = 0.5$; *blue dots* show events satisfying $\Delta T_{sr}(\mathrm{HVD}) \leq 0.5$, and *red dots* show events satisfying $\Delta T_{sr}(\mathrm{HVD}) \geq 0.5$. *Red* and *cyan vertical lines* show sunrise times at the summer solstice and the winter solstice, respectively

reversal region at reference station HVD also influenced the phase difference.

We examined the time variation of the occurrence of events in which the *D* component phase was in antiphase (a phase lag of between 90° and 270°) to more accurately compare the sharpness of the phase shift with LT and ΔT_{sr}. Figure 5 shows the LT and ΔT_{sr} dependences against the percentage occurrence of antiphase events. The percentage occurrence began to increase at LT = 3.5 or $\Delta T_{sr} = 0$, although the increase with ΔT_{sr} was sharper

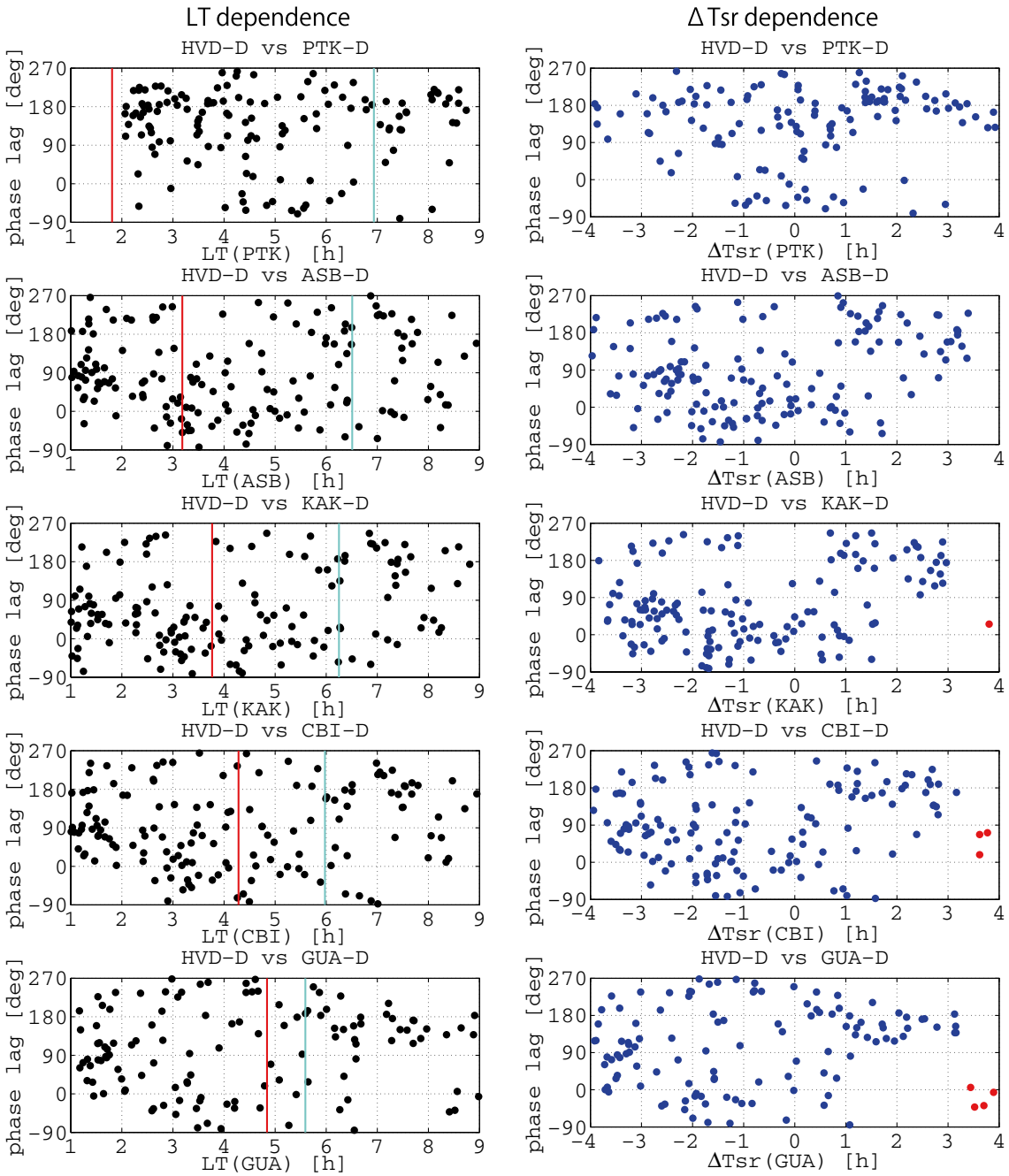

Fig. 4 LT and ΔT_{sr} dependency of the phase lag of the *D* component between HVD and the five test stations in the same format as Fig. 3

than the increase with LT. At PTK and GUA, the percentage occurrence was relatively high before the start of phase shift (~60 %), indicating that the phase was scattered.

We statistically examined the *D* component phases when the phase reversal region ($0.5 \leq \Delta T_{sr} \leq 1$) was located between HVD and each test station. The geometry of the stations and the terminator in this situation is shown in Fig. 6. Such events should satisfy $\Delta T_{sr}(\mathrm{HVD}) \leq 0.5$ and $1 \leq \Delta T_{sr}(\mathrm{STN})$, corresponding to blue dots in $1 \leq \Delta T_{sr}(\mathrm{STN})$ in Fig. 4. Table 2 gives the percentage of antiphase relation events. We used two criteria for the antiphase relation: $180° \pm 45°$ and $180° \pm 90°$. The percentage of antiphase events ranged up to 58 %

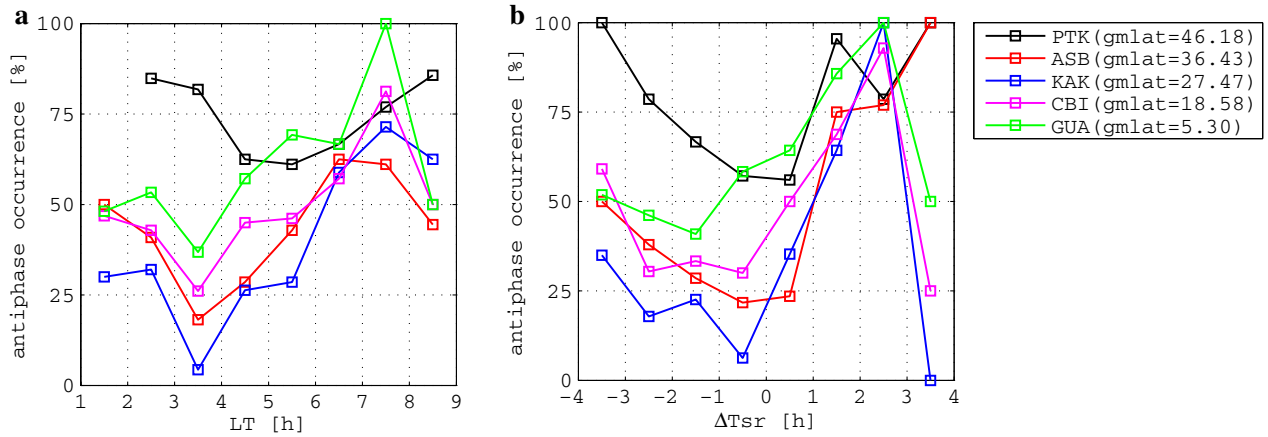

Fig. 5 **a** LT and **b** ΔT_{sr} dependency of the occurrence of antiphase events (phase lag between 90° and 270°). The percentage occurrence is given in each hourly bin

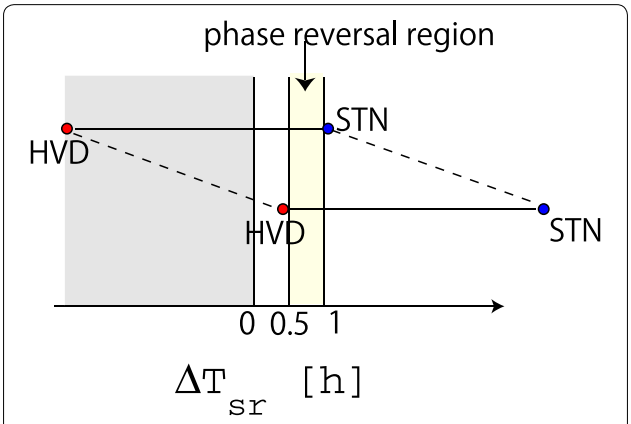

Fig. 6 Locations of HVD and each test station (STN) relative to the dawn terminator when ΔT_{sr}(HVD) ≤ 0.5 and $1 \leq \Delta T_{sr}$(STN) are satisfied

Table 2 The percentage occurrence of antiphase events when the dawn phase reversal region was located between HVD and each test station

Station	180° ± 45° (%)	180° ± 90° (%)
PTK	68	88
ASB	58	81
KAK	63	83
CBI	68	81
GUA	69	92

for 180° ± 45° and 81 % for 180° ± 90°, suggesting that *D* phase reversal occurred around the dawn terminator in most cases.

We analyzed amplitude characteristics of Pi2 around the dawn terminator. The amplitude was simply determined by the maximum perturbation of the band-pass-filtered data with a period of 40–150 s. Figure 7 shows the LT and ΔT_{sr} dependences of the *H* and *D* amplitudes and the *D*-to-*H* amplitude ratio. The *H* amplitude at ASB, KAK, and CBI decreased toward noon, although the *H* amplitude at GUA increased toward noon on the dayside, which is due to the dayside equatorial Cowling effect. The variation in the *H* amplitude at PTK was different, with a minimum appearing at LT = 3–4. This minimum may be because the *H* component in the higher latitude produced by a pair of FACs varies more sharply with longitude and its sense is reversed at a specific longitude (e.g., Bonnevier et al. 1970). The *D* amplitudes increased with latitude on both the nightside and dayside. Although Pi2s are believed to have a larger amplitude on the nightside than on the dayside, the *D* amplitude on the dawn side started to increase after sunrise. The *D*-to-*H* amplitude ratio started to increase at LT = 5 and $\Delta T_{sr} = 0$, although the increase with ΔT_{sr} was more significant than that with LT except at PTK. The *D*-to-*H* amplitude ratio of $1 \leq \Delta T_{sr} \leq 2$ at ASB was 2.2, while that of $-2 \leq \Delta T_{sr} \leq -1$ was 0.9, suggesting that the dawn side Pi2 was more polarized in the azimuthal direction in sunlight than in darkness.

Pi2 around the dusk terminator

We performed the same analysis for the dusk-side Pi2 events. Figure 8 shows the LT and ΔT_{ss} dependences of the phase lag of the *H* component between HVD and the five test stations. The color-coded dots indicate the location of the HVD station with respect to

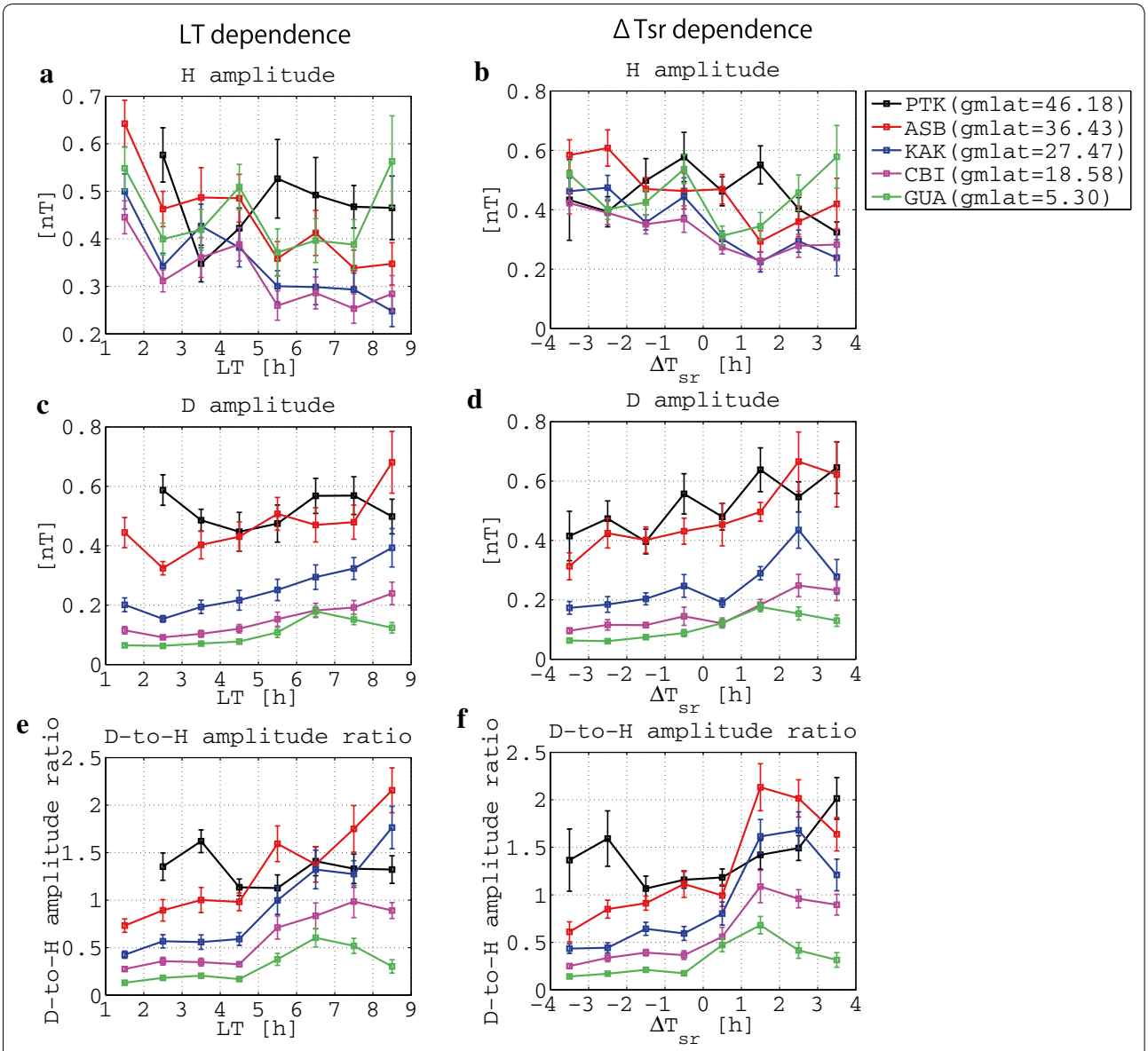

Fig. 7 LT dependency of **a** *H* amplitude, **c** *D* amplitude, and **e** *D*-to-*H* amplitude ratio and ΔT_{sr} dependency of **b** *H* amplitude, **d** *D* amplitude, and **f** *D*-to-*H* amplitude ratio. *Error bars* denote the standard errors of the mean

the $\Delta T_{ss}(\mathrm{HVD}) = -2$; blue dots show events satisfying $\Delta T_{ss}(\mathrm{HVD}) \geq -2$ and, red dots show events satisfying $\Delta T_{ss}(\mathrm{HVD}) \leq -2$. As with the dawn side, the majority phase lags were near 0° for both LT and ΔT_{ss} and for all stations except PTK. The phase lag of *H* at PTK was more scattered than that at the other stations.

Figure 9 shows the LT and ΔT_{ss} dependences of phase lag of the *D* component between HVD and the five examined stations. There was no obvious systematic change of phase with LT at any station. The phase lags at ASB, KAK, and CBI appeared to show a phase shift from ~0° to ~180° near $\Delta T_{ss} = -2$ to 1, although these were less clear than the phase shift on the dawn side. This phase reversal region was located further sunward than the corresponding region on the dawn side. After the reversal, the phase gradually decreased to ~45° with ΔT_{ss}. At PTK and GUA, there was no clear systematic change in the phase.

We examined the time variation of the occurrence of events in which the *D* component phase was in antiphase (a phase lag of between 90° and 270°) to more clearly compare the sharpness of the phase shift with the LT and ΔT_{ss}. Figure 10 shows the LT and ΔT_{ss} dependences of the percentage occurrence of antiphase events. No clear systematic change in the percentage occurrence was

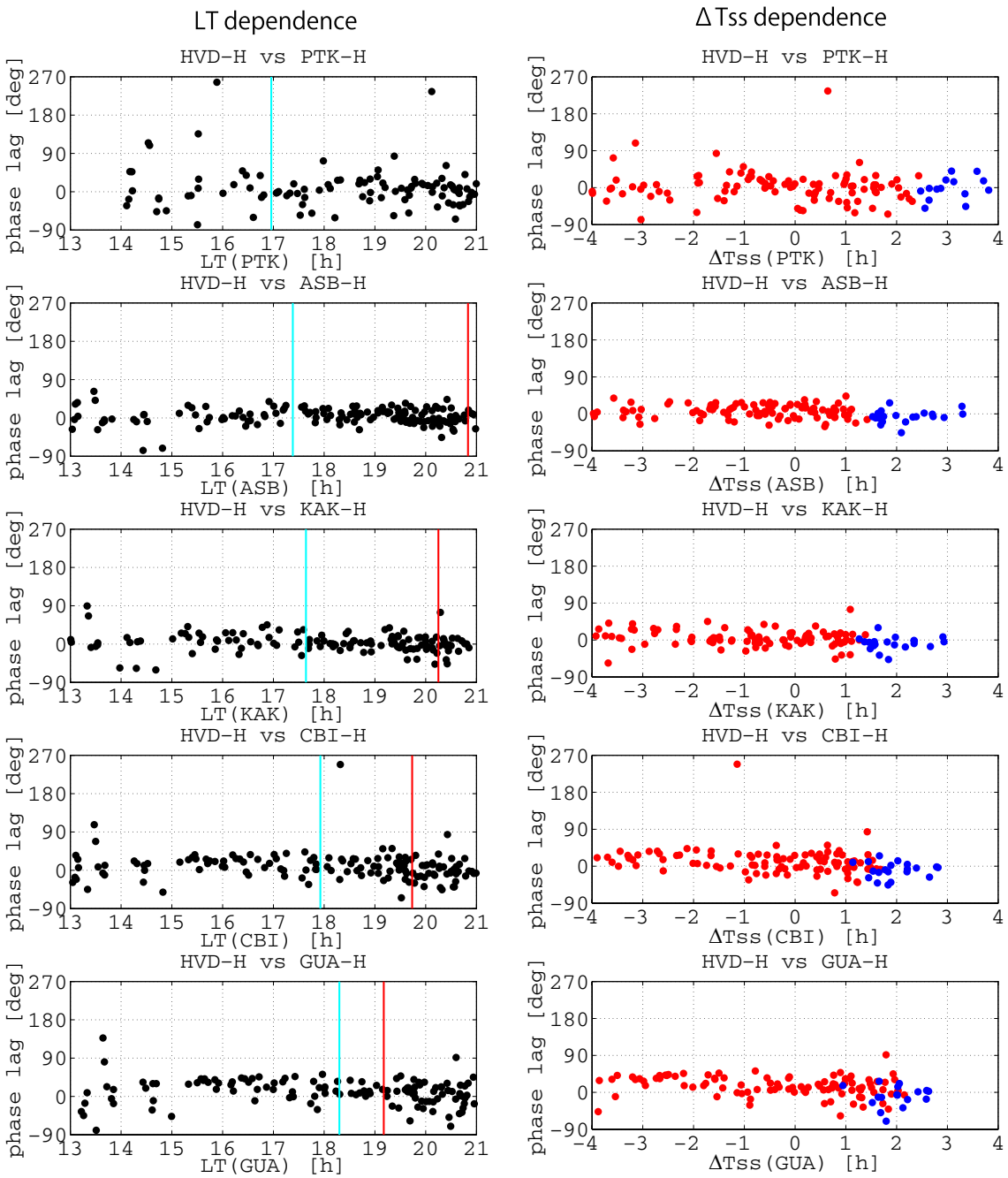

Fig. 8 LT and ΔT_{ss} dependency of the phase lag of the *H* component between HVD and the five test stations. *Positive values* indicate that the phase of the data was delayed with respect to the reference data. The *color-coded dots* indicate the location of the HVD station with respect to the ΔT_{ss}(HVD) $= -2$; *blue dots* show events satisfying ΔT_{ss}(HVD) ≥ -2 and *red dots* show events satisfying ΔT_{ss}(HVD) ≤ -2. The *red* and *cyan vertical lines* show sunset times at the summer solstice and the winter solstice, respectively

associated with LT. The percentage occurrence began to increase at $\Delta T_{ss} = -2.5$ and exceeded 75 % at $\Delta T_{ss} = -1$ to 1.

We statistically examined the *D* component phases when the phase reversal region ($-2 \leq \Delta T_{ss} \leq -1$) was located between HVD and each test station in the manner shown in Fig. 6. The events in this situation should satisfy ΔT_{ss}(HVD) ≤ -2 and $-1 \leq \Delta T_{ss}$(STN), corresponding to red dots in $-1 \leq \Delta T_{ss}$(STN) in Fig. 9. Table 3 gives the percentage of antiphase relation, which

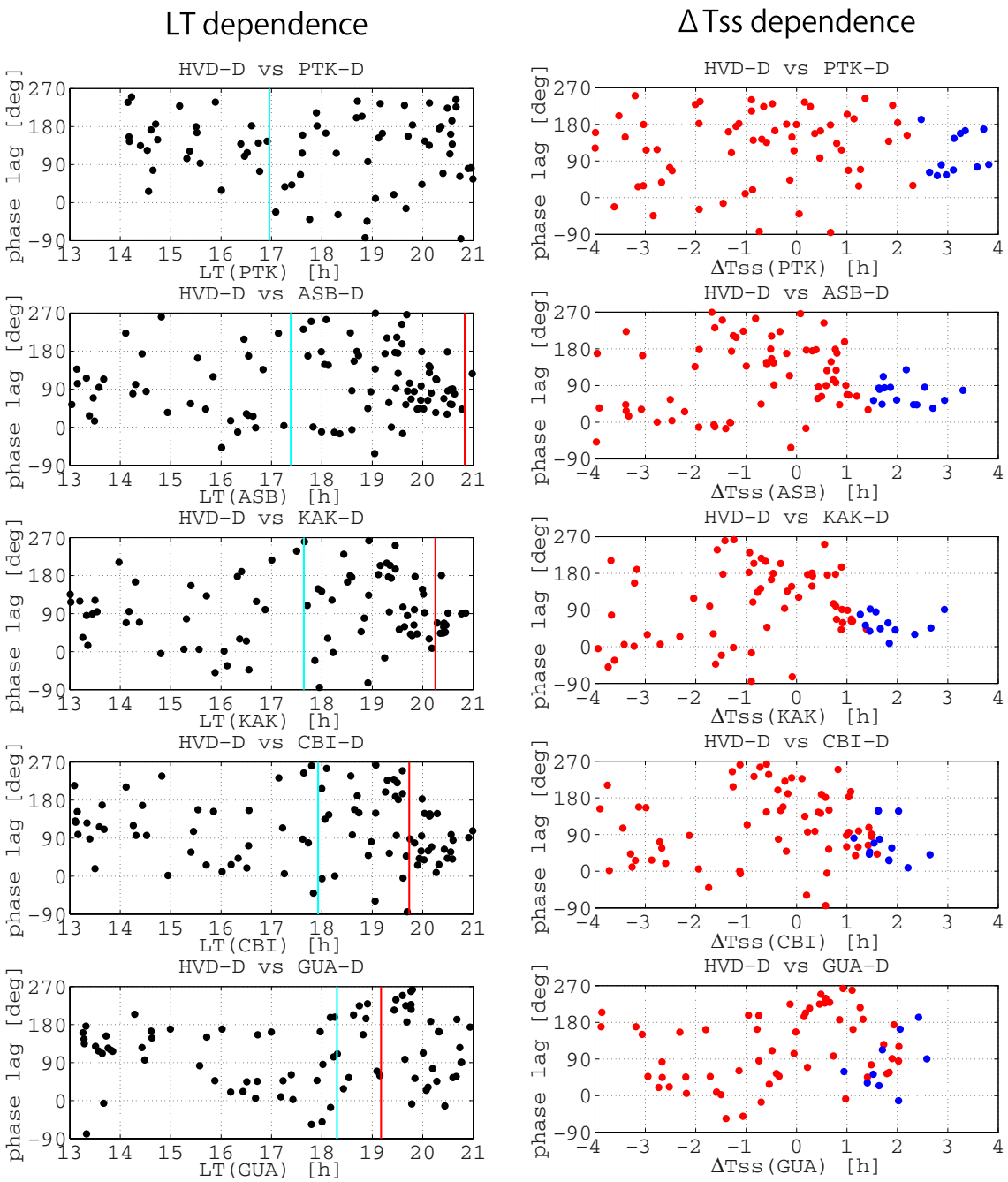

Fig. 9 LT and ΔT_{ss} dependency of the phase lag of the *D* component between HVD and the five test stations. *Positive values* indicate that the phase of the data was delayed with respect to the reference data HVD *D*. The *red* and *cyan vertical lines* show sunset times at the summer solstice and the winter solstice, respectively

ranged up to 31 % for 180° ± 45° and 68 % for 180° ± 90°. The phase lags were distributed around 180° rather than 0° although this tendency was weaker than on the dawn side.

Figure 11 shows the LT and ΔT_{ss} dependences of the *H* and *D* amplitudes and the *D*-to-*H* amplitude ratio. The *H* amplitude is largest at PTK, and its variation was different from those of the other stations. The *D* amplitude increased with latitude on both the nightside and dayside, with the increase beginning at LT = 17 toward midnight. With the exception of PTK the *D*-to-*H* amplitude ratios increased with latitude, and varied little with longitude.

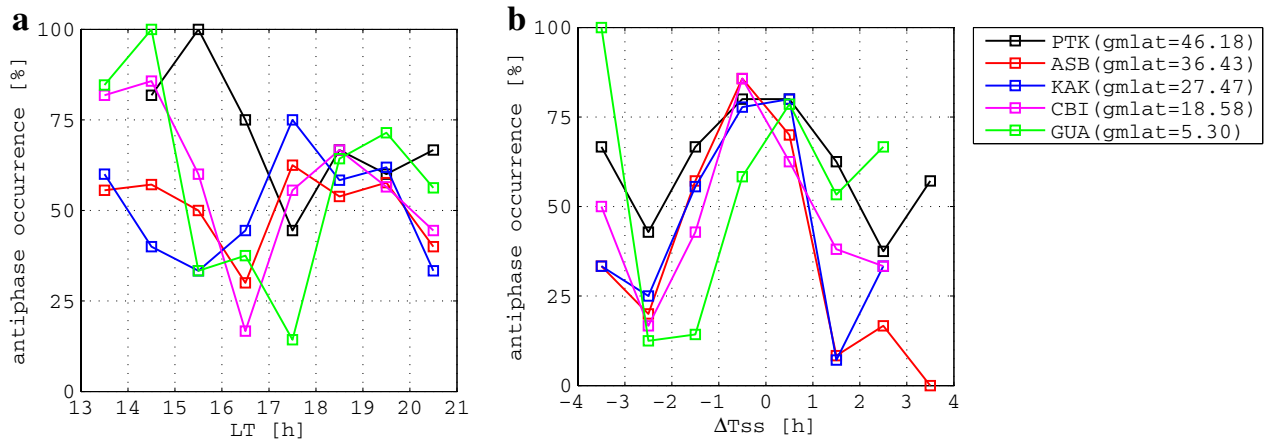

Fig. 10 **a** LT and **b** ΔT_{ss} dependency of the occurrence of antiphase events (phase lag between 90° and 270°). The percentage occurrence is given in each hourly bin

Table 3 The percentage occurrence of antiphase events when the phase dusk reversal region ($-2 \leq \Delta T_{ss} \leq -1$) was located between HVD and each test station

Station	180° ± 45° (%)	180° ± 90° (%)
PTK	50	75
ASB	42	68
KAK	45	68
CBI	32	68
GUA	37	68

However, in contrast to the dawn side, little difference was observed in the steepness of the longitudinal variations between ΔT_{ss} and LT. Peaks of *D*-to-*H* amplitude ratio occurred near LT = 19 and $\Delta T_{ss} = 0$. This differs from the *D*-to-*H* amplitude ratio on the dawn side, whose peak occurs at a few hours toward noon from the dawn terminator.

Discussion

We have shown that the phase and amplitude were structured around the dawn and dusk terminators. The key observations presented in this research are summarized in Table 4. The phase of the *H* component varied little with either the LT or sunrise/sunset reference time, which was consistent with previous observations (Kitamura et al. 1988; Nosé et al. 2003, 2006). However, the phase structure of the *D* component was not uniform. The *D* phase was reversed near the terminator, and the longitude at which the phase reversal occurred depended on the location of the terminator rather than on the LT. The phase reversal associated with the dawn terminator was substantially higher than that associated with the dusk terminator. This suggests that the longitudinal gradient of ionospheric conductivity affected the phase of the *D* component Pi2. According to Tanaka et al. (2007), the incidence of a fast mode wave toward the ionosphere near the terminator does not lead to the ionospheric current causing a *D* component phase reversal. The horizontal structure of the fast wave can be assumed to be uniform because the phase difference of *H* component is small around the terminators. The primary zonal electric field of the fast mode waves generates electric charges along the terminator, but the secondary zonal electric field is weaker than the primary field and the total electric field is in the same direction in the sunlit and dark ionospheres. The meridional Hall currents driven by the total electric field also flow in same direction between sunlight and darkness. Models based on the fast mode wave [plasmaspheric resonance (e.g., Yeoman and Orr 1989) or the direct driven fast mode wave (e.g., Kepko and Kivelson 1999)] cannot therefore explain the *D* phase reversal near the terminator. Recently Imajo et al. (2015) suggested that the terminator effect could be explained by a change in the contributing currents from the FACs on the nightside to the meridional ionospheric currents on the sunlit side of the terminator, and *vice versa*. The meridional ionospheric currents are part of the dayside ionospheric current closure, including the equatorial Cowling current (see figure 8 in the 2015 paper). In the context of the current system, we discuss the geometry of the FACs, the ionospheric currents, and the terminator on the basis of our observations.

The dawn–dusk asymmetry in the longitudinal structure of the *D*-to-*H* amplitude ratio may reflect the asymmetry of the FAC configuration and the meridional

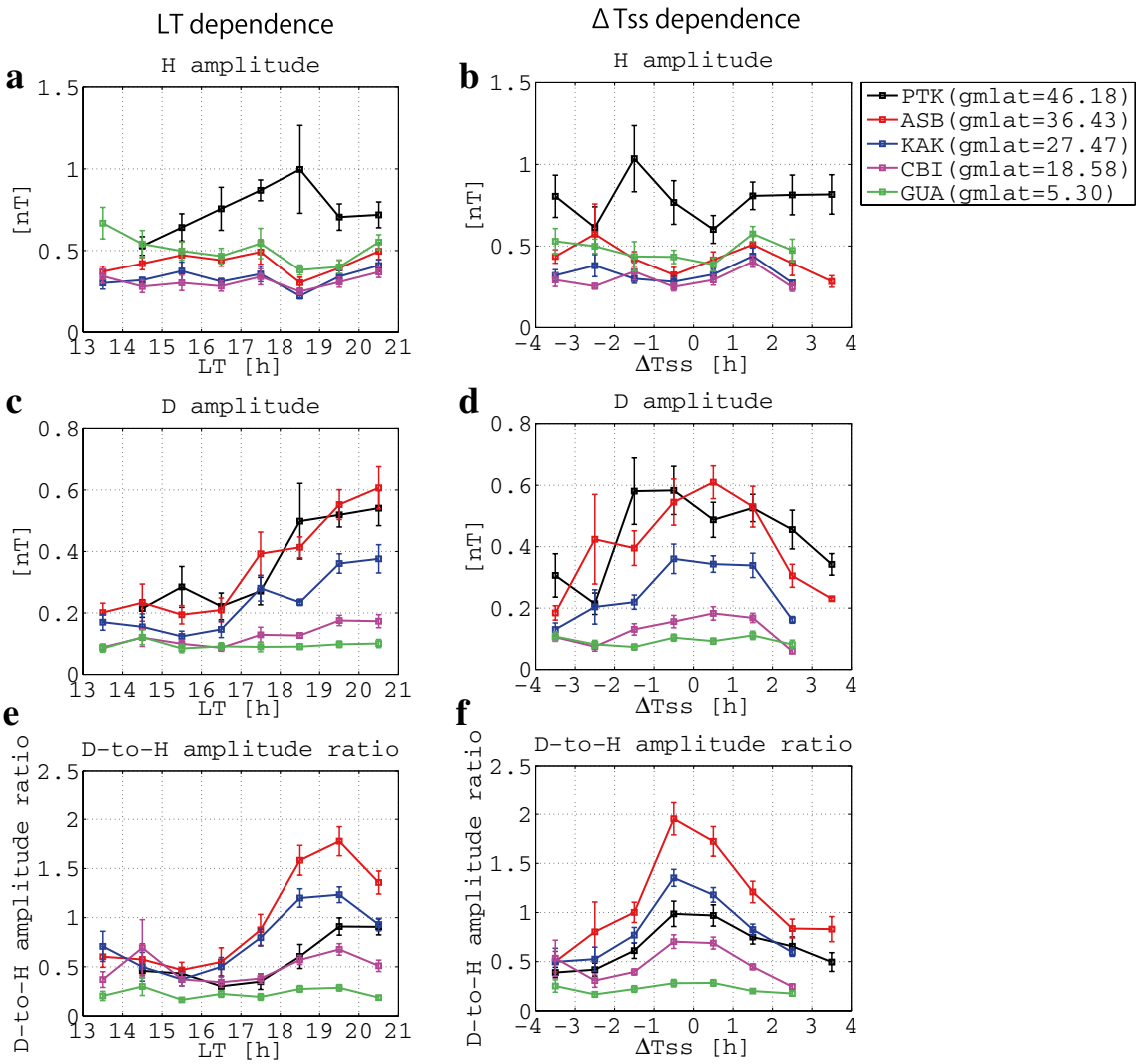

Fig. 11 LT dependency of **a** *H* amplitude, **c** *D* amplitude, and **e** *D*-to-*H* amplitude ratio and ΔT_{ss} dependency of **b** *H* amplitude, **d** *D* amplitude, and **f** *D*-to-*H* amplitude ratio

Table 4 Summary of the observations presented in this paper

	Dawn	Dusk
H phase	Almost constant; larger dispersion at middle latitude	Almost constant
D phase	Phase reversal in 0.5–1 h after sunrise; larger dispersion before the reversal at middle and very low latitudes	Phase reversal in 1–2 h before sunset at low latitudes but with weaker tendency than the dawn phase reversal; no systematic change at middle and very-low latitudes
H amplitude	Tendency to decrease toward noon but at very low latitude increase after sunrise	No clear trend
D amplitude	Increases toward noon; increases with latitude except at middle latitude	Increase begins at 17 h LT or 2 h before sunset; increases with latitude except at middle latitude
D-to-*H* amplitude ratio	Increase begins at sunrise and peaks at 2 h after sunrise except at middle latitude; increases with latitude except at middle latitude	Increase begins at 17 h LT or 2 h before sunset and peaks at 19 h LT or sunset except at middle latitude; weaker terminator dependence than the dawn terminator; increases with latitude except at middle latitude

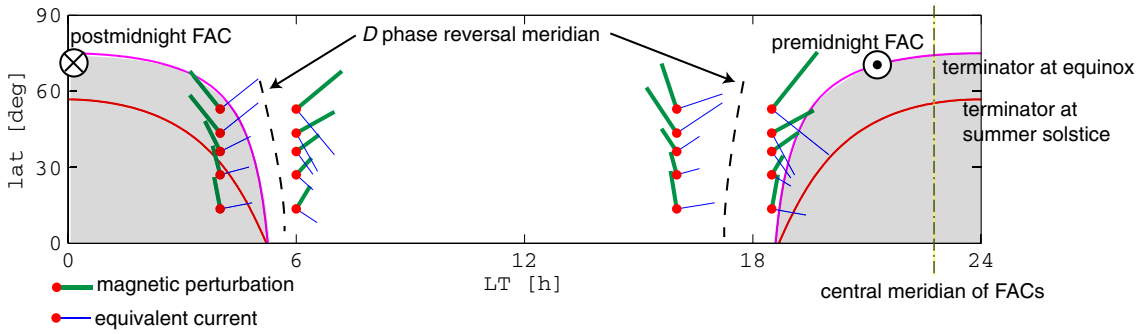

Fig. 12 Illustration of the averaged magnetic and equivalent current perturbation around the phase reversal meridians and the possible configuration of ionospheric footprints of the FACs associated with Pi2. *Magenta* and *red curves* show the terminators at 100 km in altitude at equinox and summer solstice, respectively. *Black dashed* and *dashed-dotted lines* show the *D* component phase reversal meridians and the central meridian of Pi2-associated FACs, respectively. *Green* and *blue vectors* show magnetic and equivalent current vectors, respectively, on both sides of the phase reversal meridians

ionospheric currents. Figure 12 shows the averaged magnetic and equivalent current perturbation around the phase reversal meridians and the possible configuration of ionospheric footprints of the FACs that is expected from the observational results. At this time, it is assumed that the dusk and dawn sides Pi2-associated FACs are directed upward and downward, respectively. Note that the magnetic vectors and FACs will be directed in opposite directions at the half-period of Pi2 after this time. It is thought that the magnetic perturbation produced by the FAC is stronger on the dusk side than on the dawn side because the Pi2 source, which is believed to be located at the center of Pi2-associated FACs, is on average shifted duskward (e.g., Uozumi et al. 2007). The *D*-to-*H* amplitude ratio on the sunward side of the phase reversal meridians was smaller on the dusk side than on the dawn side. Assuming that the ground Pi2 magnetic oscillation in the sunward side of the phase reversal meridians is driven mainly by the overhead ionospheric current, the equivalent current vectors (the blue vector in Fig. 12) in the sunward side will be directed in a similar direction to the overhead ionospheric current at each station. This may indicate that the meridional component of the ionospheric current is smaller on the dusk side, as predicted by Yoshikawa et al. (2012). If the magnetic effect of the FAC is stronger than that of the meridional ionospheric current on the dusk side, the location dependence of the dusk terminator is weaker than that of the Pi2-associated FACs. This is consistent with the observation that dependencies of the dusk terminator were less obvious than those of the dawn terminator. However, caution should be exercised when the equivalent current in the conductivity gradient region interpreted as ionospheric current because the equivalent current in this region can be affected by both magnetospheric and ionospheric currents.

The dawn–dusk asymmetry of the *D* component phase reversal may also be related to that of the ionospheric conductance in the auroral zone. In the evening sector, the Region 1 (R1) current flows upward (out of the ionosphere), which is very often accompanied by the precipitation of auroral electrons, and it is well known that the accelerated (mono-energetic) auroral precipitation tends to be more intense when the ionospheric footprint is dark than when it is sunlit (e.g., Newell et al. 1996). Ohtani et al. (2009) statistically examined the contributions of solar illumination and electron precipitation to the Pedersen conductance at the footprints of upward R1 currents, and they found that the ionospheric conductance actually tends to be higher in the dark hemisphere than in the sunlit hemisphere. It is therefore possible that around the dusk terminator the ionospheric conductance decreases from nightside to dayside along the auroral oval, and then it starts to increase toward dayside at an earlier local time where the solar illumination dominates electron precipitation in ionospheric ionization. In addition, because the contribution of electron precipitation to the ionospheric ionization depends on geomagnetic activity, the longitudinal profile of the ionospheric conductance may differ from event to event. Around the dawn terminator, in contrast, electron precipitation is energetic and diffuse, which does not depend on the solar illumination at the ionospheric footprint. It is therefore expected that the dawn terminator serves as a good reference for the longitudinal gradient of the ionospheric conductance. The distribution of the ionospheric conductance affects not only the ionospheric current distribution but also the FAC distribution. Thus, the conductivity distribution in the auroral region possibly affects the *D* component of low- to middle-latitude Pi2 pulsations, resulting in the dawn–dusk difference in the longitude of the *D* component phase reversal relative to

the terminator. However, it still remains to be understood how specifically the conductance gradient is physically related to the *D* component Pi2 oscillation.

The latitudinal profile of the *D* amplitude (or *D*-to-*H* amplitude ratio) was consistent with both the magnetic effect of the FACs and meridional ionospheric currents. The *D* component produced by the FACs decreased significantly more with decreasing latitude than the *H* component, because of the opposite *D* component produced by the geomagnetic conjugate FACs in the opposite hemisphere. At the sunlit side, the meridional current is thought to connect not only with the zonal Cowling current at the magnetic equator but also with the zonal current at low latitudes. Thus the meridional ionospheric current, which drives the *D* magnetic perturbations, decreases toward the magnetic equator.

Pi2 pulsations at the middle-latitude PTK showed different features from low-latitude Pi2s and were less dependent on the sunrise/sunset reference time than those at the low-latitude stations. The large annual variation of the sunrise/sunset time (approximately 5.2 h) probably produces different features and weakens the sunrise/sunset reference time dependence. At the summer solstice, the phase reversals around midnight (caused by upward and downward FACs) and the terminator (caused by an FAC and a meridional current) may mix because the dawn and dusk terminators are located near midnight (~1.6 and 22.4 h LT; see the red line in Fig. 12). Furthermore, the major axis of Pi2 polarization is easily influenced by the location of the oscillating FACs when a station is located closer to the FACs. Thus, the middle-latitude Pi2 polarization varies more significantly from event to event than the low-latitude Pi2s.

Although the uniform phase structure of the *H* component has been interpreted as evidence of a uniform global cavity mode (Sutcliffe and Yumoto 1989; Yumoto 1990; Sutcliffe and Yumoto 1991; Nosé et al. 2006), we suggest that the uniform phase structure can be explained equally well by nightside FACs and the zonal component of the dayside ionospheric current. The *H* component produced by a pair of FACs (e.g., a classical one-loop substorm current wedge McPherron et al. 1973) decreases with the distance from the central meridian of the FACs and changes direction at a specific distance (e.g., Bonnevier et al. 1970; Kisabeth and Rostoker 1977; Cramoysan et al. 1995). Assuming that the eastside FAC is downward and the westside FAC is upward, the zonal component of the dayside ionospheric closure current will be directed eastward, and consequently the *H* component near the central meridian of the FACs and on the sunlit region are positive. According to calculations by McPherron et al. (1973) and Cramoysan et al. (1995), the *H* magnetic field at 30° latitude produced by the one-loop substorm current wedge is positive in a LT sector of approximately 19–05 h. It is therefore likely that the uniform phase structure of the *H* component can be explained by the FAC and the zonal component of the dayside ionospheric current closure, although this will depend on the configuration of the FACs. However, we do not exclude the possibility that the fast mode wave also contributes to the *H* component of dawn and dusk Pi2s, as Pi2 pulsations in the compressional component have been reported in the dawn and dusk magnetosphere (Nosé et al. 2003; Kim et al. 2010).

If Pi2 pulsations are driven only by the simultaneous electrostatic current oscillation, their phase relations at different locations can be just 0° or 180°. It is not clear why some cases showed a scattered distribution or a gradual change with longitude (e.g., Fig. 9). Waters et al. (2001) showed that the vertical propagation effect in the ionosphere, which is controlled by the ionospheric conductivity, and horizontal wave number, can be a cause of the gradual phase shift with longitude of equatorial ULF waves. We suggest two other possibilities. One possibility is that the phase is changed by other Pi2 components with different phases from the electrostatic oscillation (e.g., propagating MHD waves or inductive currents). Another possibility is that the current system consists of many small-scale structures which oscillate in different phase to each other. However, at present, we cannot explain how these other Pi2 components and small structures modify the major phase structure.

Numerical modeling of the magnetic field produced by the current system should be undertaken to confirm our interpretation of the terminator effects. To study Pc pulsations, Alperovich et al. (1996) numerically simulated the equivalent current system (the rotational part of the ionospheric current system) of the current system produced by dayside FACs. The simulation showed changes in the equivalent current pattern near the dawn terminator, but these depended on the season (conductivity distribution) and the location of the FACs (incident Alfvén wave). No numerical study has produced the magnetic field (or equivalent current) near the terminator produced by the nightside source current system, and the contributions of FACs and ionospheric currents have not been separately examined.

Conclusions

The local time (LT) and sunrise/sunset reference time dependences of Pi2 pulsations observed at middle- to low-latitude stations around the dawn and dusk terminators were examined. A statistical analysis using Pi2 events that occurred between November 1, 2011 to October 31, 2012, showed that some features of the Pi2s were controlled by

the relative location of the terminator (at 100-km altitude, where the highly conducting *E* region is located) rather than by the local time. A summary of observational results is shown in Table 4. The terminator effects can be explained by a change in the contributing currents, in particular of the FACs on the nightside to the meridional ionospheric currents on the sunlit side of the terminator and *vice versa*. Based on the dayside ionospheric current closure of the nightside FACs (Yoshikawa et al. 2012; Imajo et al. 2015), we suggest the following conclusions:

The asymmetry of the dawn–dusk features suggests that the magnetic contribution of the nightside FAC relative to the meridional ionospheric current is stronger on the dusk side than that on the dawn side, implying that the center of the Pi2-associated FACs, which probably corresponds to the Pi2 energy source, is shifted duskward on average, and the meridional ionospheric current is weaker on the dusk side than on the dawn side.

The azimuthal magnetic field produced by the FACs in darkness and by the meridional ionospheric current in sunlight decreases with decreasing latitude.

The different features and weak sunrise/sunset reference time dependences at the middle-latitude station can be attributed to a larger annual variation of the sunrise/sunset time and a stronger magnetic effect of the FACs.

The uniform phase structure of the *H* component can be explained either by a global cavity mode or by the FAC and the zonal component of dayside ionospheric current closure; however, this depends on the configuration of the FACs.

It is not clear why cases are observed wherein the phases are not distributed around 0°/180° or change gradually. Other Pi2 components and small-scale structures may be associated with shifts in phase. The dawn–dusk asymmetric current system comprising nightside FACs and dayside ionospheric current closure is qualitatively consistent with the terminator effects on Pi2 pulsations. However, numerical modeling of the magnetic field produced by the current system should be conducted in order to confirm our interpretation. We will undertake such a numerical analysis in a future study.

Authors' contributions

SI analyzed the data and drafted the manuscript. AY, TU, SO, and AN made substantial contributions to the interpretation of data and revision of the draft manuscript. SD and BMS made substantial contributions to the acquisition of MAGDAS magnetic data. All authors read and approved the final manuscript.

Author details

[1] Department of Earth and Planetary Sciences, Kyushu University, 744 Motooka, Nishi-ku, Fukuoka 819-0395, Japan. [2] International Center for Space Weather Science and Education, Kyushu University, Motooka, Nishi-Ku, Fukuoka 819-0395, Japan. [3] The Johns Hopkins University Applied Physics Laboratory, 11100 Johns Hopkins Rd., Laurel, MD 20723, USA. [4] Applied Electromagnetic Research Institute, National Institute of Information and Communications Technology, 4-2-1 Nukui-Kitamachi, Koganei, Tokyo 184-8795, Japan. [5] Institute of Astronomy and Geophysics, Mongolian Academy of Sciences, Maakhuur Tolgoi, BZD, Lkhagvasuren Street-42, Ulaanbaatar 13343, Mongolia. [6] Institute of Cosmophysical Researches and Radio Wave Propagation, 7 Mirnaya St., v. Paratunka, Elizovskiy Region, Kamchatka, Russia 684034.

Acknowledgements

This work was supported in part by JSPS Core-to-Core Program, B. Asia-Africa Science Platforms, by Grant-in-Aid for JSPS Fellows (15J02300), and by JSPS KAKENHI (15H05815). The magnetic data from KAK and CBI are provided by JMA, TAM are provided by BCMT, and GUA and TUC are provided by USGS. MAGDAS magnetic data from ASB are supported by Mr. Koji Nosakon. The authors would like to thank Enago (www.enago.jp) for the English language review.

Competing interests

The authors declare that they have no competing interests.

Received: 26 March 2016 Accepted: 20 July 2016
Published online: 02 August 2016

References

Allan W, Menk FW, Fraser BJ, Li Y, White SP (1996) Are low-latitude Pi2 pulsations cavity/waveguide modes? Geophys Res Lett 23(7):765–768. doi:10.1029/96GL00661

Alperovich L, Fidel B, Saka O (1996) A determination of the hydromagnetic waves polarization from their perturbations on the terminator. Ann Geophys 14(6):647–658. doi:10.1007/s00585-996-0647-9

Bonnevier B, Boström R, Rostoker G (1970) A three-dimensional model current system for polar magnetic substorms. J Geophys Res 75(1):107–122. doi:10.1029/JA075i001p00107

Chi PJ, Russell CT, Ohtani S (2009) Substorm onset timing via traveltime magnetoseismology. Geophys Res Lett. doi:10.1029/2008GL036574

Cramoysan M, Bunting R, Orr D (1995) The use of a model current wedge in the determination of the position of substorm current systems. Ann Geophys 13(6):583–594. doi:10.1007/s00585-995-0583-0

Imajo S, Yoshikawa A, Uozumi T, Ohtani S, Nakamizo A, Marshall R, Shevtsov BM, Akulichev VA, Sukhbaatar U, Liedloff A, Yumoto K (2015) Pi2 pulsations observed around the dawn terminator. J Geophys Res Space Phys 120(3):2088–2098. doi:10.1002/2013JA019691

Jacobs JA, Kato Y, Matsushita S, Troitskaya VA (1964) Classification of geomagnetic micropulsations. J Geophys Res 69(1):180–181. doi:10.1029/JZ069i001p00180

Keiling A, Marghitu O, Vogt J, Amm O, Bunescu C, Constantinescu V, Frey H, Hamrin M, Karlsson T, Nakamura R, Nilsson H, Semeter J, Sorbalo E (2014) Magnetosphere–ionosphere coupling of global Pi2 pulsations. J Geophys Res Space Phys 119(4):2717–2739. doi:10.1002/2013JA019085

Kepko L, Kivelson M (1999) Generation of Pi2 pulsations by bursty bulk flows. J Geophys Res 104(A11):25021–25034. doi:10.1029/1999JA900361

Kim K-H, Kwon H-J, Lee D-H, Jin H, Takahashi K, Angelopoulos V, Bonnell JW, Glassmeier KH, Park Y-D, Sutcliffe P (2010) A comparison of THEMIS Pi2 observations near the dawn and dusk sectors in the inner magnetosphere. J Geophys Res 115:A12226. doi:10.1029/2010JA016010

Kisabeth JL, Rostoker G (1977) Modelling of three-dimensional current systems associated with magnetospheric substorms. Geophys J Int 49(3):655–683. doi:10.1111/j.1365-246X.1977.tb01310.x

Kitamura T, Saka O, Shimoizumi M, Tachihara H, Oguti T, Araki T, Sato N, Ishitsuka M, Veliz O, Nyobe JB (1988) Global mode of Pi2 waves in the equatorial region: difference of Pi2 mode between high and equatorial latitudes. J Geomagn Geoelectr 40:621–634. doi:10.5636/jgg.40.621

Lester M, Hughes JW, Singer HJ (1983) Polarization patterns of Pi2 magnetic pulsations and the substorm current wedge. J Geophys Res 88(A10):7958–7966. doi:10.1029/JA088iA10p07958

McPherron RL, Russell CT, Aubry MP (1973) Satellite studies of magnetospheric substorms on August 15, 1968: 9. Phenomenological model for substorms. J Geophys Res 78(16):3131–3149. doi:10.1029/JA078i016p03131

Newell PT, Meng C-I, Lyons KM (1996) Suppression of discrete aurorae by sunlight. Nature 381:766. doi:10.1038/381766a0

Nosé M, Takahashi K, Uozumi T, Yumoto K, Miyoshi Y, Morioka A, Milling DK, Sutcliffe PR, Matsumoto H, Goka T, Nakata H (2003) Multipoint

observations of a Pi2 pulsation on morningside: the 20 September 1995 event. J Geophys Res 108(A5):1219. doi:10.1029/2002JA009747
Nosé M, Liou K, Sutcliffe PR (2006) Longitudinal dependence of characteristics of low-latitude Pi2 pulsations observed at Kakioka and Hermanus. Earth Planets Space 58:775–783. doi:10.1186/BF03351981
Ohtani S, Wing S, Ueno G, Higuchi T (2009) Dependence of premidnight field-aligned currents and particle precipitation on solar illumination. J Geophys Res 114(A12):A12205. doi:10.1029/2009JA014115
Saito T (1964) Mechanisms of geomagnetic continuous pulsations and physical states of the exosphere. J Geomagn Geoelectr 16(2):115–151
Saka O, Alperovich L (1993) Sunrise effect on dayside pc pulsations at the dip equator. J Geophys Res 98(A8):13779–13786. doi:10.1029/93JA00730
Saka O, Iijima TJ, Kitamura T (1980) Ionospheric control of low latitude geomagnetic micropulsations. J Atmos Terr Phys 42(5):517–520. doi:10.1007/BF00203620
Saka O, Itonaga M, Kitamura T (1982) Ionospheric control of polarization of low-latitude geomagnetic micropulsations at sunrise. J Atmos Terr Phys 44(8):703–712. doi:10.1016/0021-9169(82)90132-5
Saka O, Kitamura T, Shimuizumi M, Araki T, Oguti T, Veliz O, Ishitsuka M (1988) The effects of non-uniform ionosphere on the equatorial Pc pulsations. J Geomagn Geoelectr 40(5):635–643. doi:10.5636/jgg.40.635
Sastry TS, Sarma YS, Sarma SVS, Narayan PVS (1983) Day-time Pi pulsations at equatorial latitudes. J Atmos Terr Phys 45:733
Shinohara M, Yumoto K, Yoshikawa A, Saka O, Solovyev SI, Vershinin EF, Trivedi NB, Costa JMD (1997) Wave characteristics of daytime and nighttime Pi 2 pulsations at the equatorial and low latitudes. Geophys Res Lett 24:2279–2282. doi:10.1029/97GL02146
Shinohara M, Yumoto K, Hosen N, Yoshikawa A, Tachihara H, Saka O, Kitamura T-I, Trivedi NB, Costa JMD, Schuch NJ (1998) Wave characteristics of geomagnetic pulsations across the dip equator. Geophys Res Lett 103(A6):11745–11754. doi:10.1029/97JA03067
Sutcliffe PR, Yumoto K (1989) Dayside Pi2 pulsations at low latitudes. Geophys Res Lett 16(8):887–890. doi:10.1029/GL016i008p00887
Sutcliffe PR, Yumoto K (1991) On the cavity mode nature of low-latitude Pi2 pulsations. J Geophys Res 96(A2):1543–1551. doi:10.1029/90JA02007
Tanaka Y-M, Yumoto K, Yoshikawa A, Shinohara M, Kawano H, Kitamura T-I (2004) Longitudinal structure of Pc3 pulsations on the ground near the magnetic equator. J Geophys Res 109(A3):A03201. doi:10.1029/2003JA009903
Tanaka Y-M, Yumoto K, Yoshikawa A, Itonaga M, Shinohara M, Takasaki S, Fraser BJ (2007) Horizontal amplitude and phase structure of low-latitude Pc 3 pulsations around the dawn terminator. J Geophys Res 112(A11):A11308. doi:10.1029/2007JA012585
Uozumi T, Yumoto K, Kawano H, Yoshikawa A, Olson JV, Solovyev SI, Vershinin EF (2000) Characteristics of energy transfer of Pi2 magnetic pulsations: latitudinal dependence. Geophys Res Lett 27(11):1619–1622. doi:10.1029/1999GL010767
Uozumi T, Kawano H, Yoshikawa A, Itonaga M, Yumoto K (2007) Pi2 source region in the magnetosphere deduced from CPMN data. Planet Space Sci 55:849–857. doi:10.1016/j.pss.2006.03.016
Waters CL, Sciffer MD, Fraser BJ, Brand K, Foulkes K, Menk FW, Saka O, Yumoto K (2001) The phase structure of very low latitude ULF waves across dawn. J Geophys Res 106(A8):15599–15607. doi:10.1029/2000JA000339
Welch PD (1967) The use of fast Fourier transform for the estimation of power spectra: a method based on time averaging over short, modified periodograms. IEEE Trans Audio Electroacoust 15(2):70–73. doi:10.1109/TAU.1967.1161901
Yanagihara K, Shimizu N (1966) Equatorial enhancement of micro-pulsation pi-2. Mem Kakioka Mag Obs 12:57–63
Yeoman T, Orr D (1989) Phase and spectral power of mid-latitude Pi2 pulsations: evidence for a plasmaspheric cavity resonance. Planet Space Sci 37(11):1367–1383. doi:10.1016/0032-0633(89)90107-4
Yoshikawa A, Ohtani S, Nakamizo A, Uozumi T, Tanaka Y-M (2012) Formation of Cowling channel from polar to equatorial ionosphere. Abstract SM13C-06 presented at 2012 AGU fall meeting, San Francisco, CA, 3–7 December
Yumoto K (1990) Evidences of magnetospheric cavity Pi2 waves. J Geomagn Geoelectr 42(11):1281–1290. doi:10.5636/jgg.42.1281
Yumoto K, the MAGDAS Group (2006) MAGDAS project and its application for space weather. In: Gopalswamy N, Bhattacharya A (eds) Solar influence on the heliosphere and earth's environment: recent progress and prospects. Wheaton, Quest Publications, pp 399–405
Yumoto K, the MAGDAS Group (2007) Space weather activities at SERC for IHY: MAGDAS. Bull Astron Soc India 35:511–522